Magneto Propulsive Solar Aircraft Engine

Chandrashekar[1], Dr. Chikanna N[2], Sanjeev G Palekar[3], Prashanth Radhakrishnan[4]

[1]P.G. Student, [2]Associate Professor & Chairman, [3]Assistant Professor, [4]Director-Aerospace R & D,
[1-3]Department of Aerospace Propulsion Technology,
Visvesvaraya Technological University-Centre for Post Graduate Studies, Bengaluru Region,VIAT, Muddenahalli, Chikkaballapura, Karnataka, India.
[4]Dautya Aerospace Pvt Ltd, Bengaluru, Karnataka, India.

---***---

Abstract - *The scope for electric vehicles growing rapidly now a day. There are many reasons behind the requirement for the development of electric vehicles such as fuel cost, air pollution due to emissions, fuel availability. In similar manner considering the current aviation industry, the aviation has developed a lot. However, there are many challenges the industry needs to be faced such as fuel consumption, cost of the fuel and air pollution due to emissions caused by gas turbine engines on environment. Since fuel cost, fuel availability and consumption are the major problems in current aviation industries, electric aviation may help in this. But as we know, in the current technology only a propeller driven by a motor to produce thrust will be used as an electrical engine, and there is no air breathing electrical engine exists. For a better propulsion technology, we propose here a concept of 'Magneto Propulsive Solar Aircraft Engine' to achieve pollution less aviation environment. In this work, an exterior rotor motor is designed and viewed in the point of an embedded engine for the hub of a designed ducted propeller. This configuration is designed along with a normal shaft driven ducted propeller and performance of both the configurations are analyzed and compared for power consumption, torque demanded and inertial aspects and the new concept of embedded motor propulsion technique is introduced for lightweight electric and solar aircrafts as 'Magneto Propulsive Solar Aircraft Engine'.*

Key Words: Electrification techniques, Brushless motor, Torque extraction, 3D Printing, Computational simulation, Rotor and Stator configuration, Input DC current, Output power, Cogging torque, Phase current, Magnetic flux density, Solar propulsion, Mass flow rate, Propeller drive configurations, Free stream conditions etc.

1. INTRODUCTION

Commercial aviation has become a great importance of today's aviation industry. Along with the evolving aviation industries, the air traffic has become a major part since jetliners. The current aviation industries are facing the dominant challenges that include aerodynamic noise, climate change due to emissions and decreased local air quality because of higher air traffic. Since commercial airliners breath using fossil fuels, the impact of emissions by the aviation on environment is quite greater. Due to increased air traffic, anthropogenic emissions of the aviation have led to environmental climate change and surfacewarming. Since emissions are mainly because of gas turbine engines, electrification of civil aviation is quite helpful to reduce these impacts on environment.

Overviewing current electrification techniques, the all – electric and hybrid electric or turboelectric types of electrifications are introduced. In these electric propulsion techniques, an aircraft is propelled by means of a propeller which is driven through a motor through by a controller. For the power supply batteries are used in an all – electric types of aircraft whereas in a turboelectric aircraft the battery is recharged through small gas turbine engines.

The purpose of this work is to introduce a motor embedded propeller system, instead of using a motor and a shaft – mounted propeller to drive an electric aircraft. The motor in an electric aircraft plays a major role through its performance, weight, speed, torque and especially rotor inertia. Since the rotor inertia is capability to resist the speed change OF the motor because of external load variation, this makes the rotor inertia as a significant property. Since there are many configurations of rotor exist for a radial flux motor such as outer rotor and inner rotor, the contribution of rotor inertia varies for each configuration type. Since inertia is a mass – dependent property, increasing mass can reduce the performance of the aircraft. Hence designing a motor having high rotor inertia with less weight is a challenging task to get better performance. As a solution to this, instead of using an interior rotor or shaft – mounted propeller system as a propulsion technique, an exterior rotor motor embedded propeller is introduced as objective of this work.

Nowadays, Brushless and PMSM motors were taking place a large applicative opportunity in every automotive and aerospace industries because of its advantages such as light weight, high efficiency, lower or needs no maintenance compared to other motor types. However, because of electric aircraft needs a lightweight, higher efficiency motor, a brushless or PMSM motor is found to be a good choice. Since the intension of this work is also to consider solar powered aircrafts, motor characteristics was chosen oriented to this.

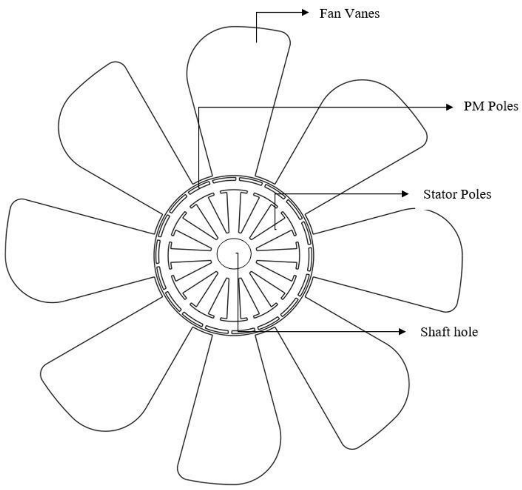

Fig-1: Representation of a schematic Propulsion System

A Hybrid propulsive engine is a general technique proposed as modified approach to the current electric aircraft propulsion system. As the system consist of an embedded exterior rotor motor, a simple lightweight square wave excited 3 phase brushless direct current motor is designed first using Ansys Rmxprt and steady state, transient performance was analyzed for expected torque and power characteristics. Since the use of sensors in the motor can be affected by the surrounding temperature, a sensor-less control was assumed during the process. Then, by using designed motor configuration, an axial fan was designed such that the whole system contributes to a motor embedded propeller as shown in Figure 1.2. Further, flow analysis is done on the shaft mounted fan and the motor embedded fan to analyze the advantages of integrating exterior rotor to axial fan vanes instead of using a shaft mounted fan. The conclusion is approached by considering the performance of the motor needed to achieve a specific flight in both the cases.

2. DIFFERENT ELECTRIFICATION TECHNIQUES

There are many electrification techniques has been introduced such as all – electric, hybrid electric and turboelectric aircrafts. The general propulsion techniques behind these electrification techniques have been understood by referring to sufficient number of scientific publications. Then the idea of embedded motor propeller driving concept has been verified by referring to current motor technologies in aviation industry.

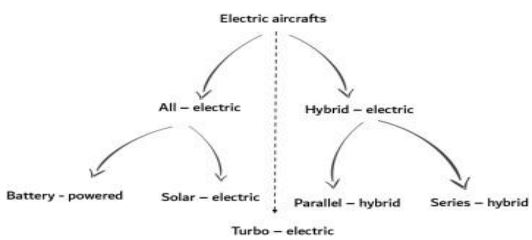

Fig-2: Different types of aircraft electrifications

3. DESIGN OF BRUSHLESS MACHINE

The brushless and PMSM type of DC or AC excited electromagnetic machines are of higher scope in current days because of its light weight, high efficiencyand smoother quality performance during operation. This will be attracted by current electric aviation because of its efficient characteristics. The difference between an exterior – rotor and interior – rotor type of motor configurations has been noted. Then based on the study, an outrunner motor is designed in Ansys maxwell environment in orientation with light weight and solar propelled aircrafts. The designed motor has been analyzed for its performance characteristics in steady and transient states.

4. DESIGNING A PROPELLER

Based on the characteristic output by the designed motor such as power output, rotational speed and maximum torque, A ducted propeller has been designed by considering power input as rated power output by the designed electromagnetic machine. The analytical design of ducted propeller is made with the help of Python 3.8 environment by considering theoretical aspects from blade element moment theory. With the same blade configuration, the designed embedded motor ducted propeller is remodeled for shaft driven one. Then the propeller duct has been designed identically for both configurations.

5. TORQUE EXTRACTION BY CFD

Since the freestream flow conditions during flight were not always same, the propeller experiences the airflow with variational load conditions acting on it throughout the flight. Hence with a considerable amount of freestream turbulence, both the ducted propellers have been solved in SolidWork's Flow simulation environment to get accurate torque demanded by both the configurations. And then the extracted torque is compared among the both configurations to achieve a suitable conclusion.

6. COMMENCEMENT

When the objective of an designing an aircraft is to reduce the kerb weight and hence to increase the payloadcapability, the weight of every component has to be reduced by an amount. When considered a fan, the weight should be minimized and thrust capability of the fan should be increased in point of view with increasing payloadcapability of the whole aircraft. By considering inertia of the fan, the fan having larger inertia can be resistant to rotational speed variation when subjected to variable loading conditions due to flow field. In other words, a fan having higher mass or larger hub can be more resistant to speed change compared to the fan with less mass or smaller hub.

7. CORE MATERIAL SELECTION

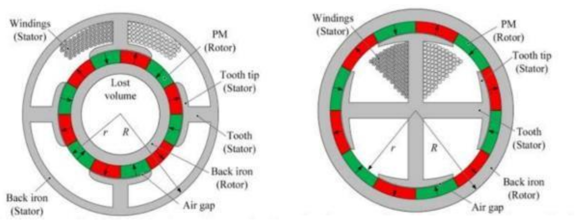

Fig-3: Different Rotor configurations

In shaft mounted fan or a propeller, the speed variation has a contribution with the rotor inertia of the motor and the self-inertia of the fan. This in turn demands a higher inertia of the rotor for smoother propulsion while operating with variable external loading. As a solution to this one can choose a motor with higher rotor inertia and higher torque. While considering an interior rotor motor, since the rotor mounted interior to the stator windings, the only option is to extend the rotor to a shaft for mounting of a propeller or a fan. But while considering an external rotor motor, since the exterior body of the motor rotates, one can vary the rotor inertia by adding or removing material on the rotor. This will createan opportunity to obtain required torque by having regulation on rotor inertia. Since the position of the rotor in an outrunner motor is made inside out, the diameter of the rotor is increased. Because of the inertia is a diameter dependent property, it will be increased for an exterior rotor motor when compared with an inrunner motor with same performance characteristics.

8. PERMANENT MAGNET SELECTION

The choice of permanent magnet depends on its Working Temperature range, Radiation Sensitivity and the property which shows resistance to the Corrosion. Since reference to the temperature is more important in this application, the PM having higher Curie temperature has been selected. The Samarium – Cobalt (SmCo) magnets the curie temperature is around 800^{0}C as observed, while for the Neodymium – Boron (NdFeB) magnets it is around 330^{0}C. As a result, the SmCo28 is selected as a magnet grade which has Curie temperature of 750^{0}C-820^{0}C and maximum working temperature of 300^{0}C. The properties of selected magnet grade are listed in below table.

Properties	Value
RFD: Relative Flux Density (T)	1.07
Force of Coercion (A/m)	820000
Energy Density Maximum (J/m3)	219350
Recoil Permeability Relative	1.03842
Density of Demagnetized Flux (T)	653076
Remanence (T) (T)	1.05

Table-1: SmCo28 magnetic properties

While choosing a magnetic core material, the core losses should be taken into account. Since the core losses have a direct impact on the motor's effectiveness, it should be less for chosen core material. For a 3-phase stator, if the No. of Magnetic Poles increase, then fundamental Electrical-Frequency also increases with respect to chosen no. of poles. And if the Frequency which to be supplied is a higher value, the core losses of the stator and yoke material increases. Hence the material should be chosen by taking all these approaches into consideration. The material properties of the chosen core material 10JNEX900 are given in below table with the core losses at different frequencies.

Parameters			
Coil pitch	1	Tooth width	18 mm
Stator outer radius	220 mm	Rotor inner diameter	222 mm
Stator inner ring diameter	182 mm	Rotor's outer diameter	248 mm
length of the back iron	7 mm	Pole embrace	0.8
Slot depth	19 mm	Slot fill factor	0.7
Average slot width	8 mm	Slot opening width	3 mm
Number of poles	20	Number of slots	24
Magnet thickness	6 mm	Airgap length	1 mm

Table-2: Properties of 10JNEX900 electrical steel

9. MAGNETIC POLE COUNT

The primary aspect is that the pole number depends on the applied fundamental square wave or sine wave frequency and required rated speed. Illustratively if the number of PM poles in a typical 16kW machine is two, then in order to operate it with 100 rotations per minute, the machine should be excited with a frequency of 2Hz. If number of poles increases the frequency of excitation increases drasticallyas per the relation with required speed shown below.

$$f = \frac{p}{4\pi}\omega_m$$

Also, when it comes to the Higher Pole Counts, then stator Magnetic Flux through each Poles can be reduced and hence the thinner ferromagnetic materials for the yoke can be selected which also in turn reduces the weight of the machine. To choose a particular pole count number of iterations with different pole and slot combinations were tried in FEM solver by considering the conceptual effects, and by observing the performance output a specific pole – slot combination is chosen for the machine.

10. ROUGH SIZING ESTIMATION

In order to design and analyze an electromagnetic machine in FEM environment, initial input parameters were necessary. Therefore, first the machine geometrical parameters were conceptually predicted owing to the desired characteristics listed in Table 5.3, and then these parameters will be obtained as optimized results by the FEM solver.

Parameters	Value
Rated speed	2300 rpm
Rated power	13kW
Efficiency	> 85%
Number of phases	3

Table-3: Desired motor characteristics

The mechanical output power by the machine depends othe mechanical speed and torque output, which can be represented as, $P = T\,\omega_m$.

As an electromagnetic machine converts the electrical power input to mechanical power, the torque output by the machine is electrically dependent on the given electrical loading q and the magnetic loading Bg for considered size of the machine. And this relationship for a square wave excited machine can be represented as,

$$T = \frac{\pi}{\sqrt{6}}\, q\, B_g\, D_{so}^2\, L$$

For a desired torque output, assuming the magnetic and electric loading, the stator outer diameter and stack length of the machine can be obtained.

The electrical loading of the machine depends on the current density in the slot winding, and the torque output by the machine is directly depends on the current density, if higher torque is required then by increasing number of turns and current through the slot winding increases the torque, alternatively, decreasing the slot area can also increases the current density as a consequence the torque. The current density dependent electrical loading can be expressed as,

$$q = h_s\, J\, k_{cu}\, w_s/(w_s+w_t)$$

where h_s indicates the height of slot, J is current density, K_{cu} is copper slot fill factor, The stator's tooth width is wt, whereas the slot width is w_s.

Parameters	Value	Parameters	Value
Coil pitch	1	Tooth width	18 mm
Stator outer radius	220 mm	Rotor inner diameter	222 mm
Stator inner ring diameter	182 mm	Rotor's outer diameter	248 mm
length of the back iron	7 mm	Pole embrace	0.8
Slot depth	19 mm	Slot fill factor	0.7
Average slot width	8 mm	Slot opening width	3 mm
Number of poles	20	Number of slots	24
Magnet thickness	6 mm	Airgap length	1 mm

Table-4 : Analytical results of designed motor

To reduce unknowns, here the Width of the Slot is considered same as the tooth width of the stator, and while analyzing the motor in FEM solver these values were optimized to a desired value of ratings. A Python program was built to solve for the sizing parameters of the motor using magnetic circuit method and the results obtained has shown in below table.

11. COMPUTATIONAL SIMULATION

The parameters listed in Table 5.4 are used for modelling the design in Ansys Rmxprt. The model created using these parameters is solved first and results were analyzed then by observing the output results by the solver, the dimensions of the machine are modified to optimal value to get efficient results. The optimized model is analyzed by Maxwell 2D for flux density distribution and other transient performance characteristics.

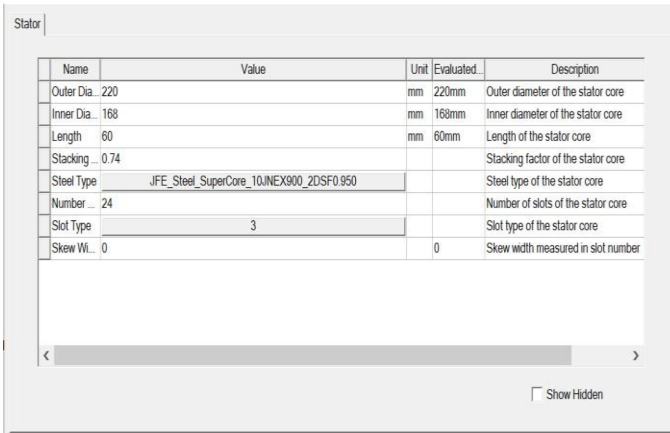

Stator

Name	Value	Unit	Evaluated...	Description
Outer Dia...	220	mm	220mm	Outer diameter of the stator core
Inner Dia...	168	mm	168mm	Inner diameter of the stator core
Length	60	mm	60mm	Length of the stator core
Stacking ...	0.74			Stacking factor of the stator core
Steel Type	JFE_Steel_SuperCore_10JNEX900_2DSF0.950			Steel type of the stator core
Number ...	24			Number of slots of the stator core
Slot Type	3			Slot type of the stator core
Skew Wi...	0		0	Skew width measured in slot number

Show Hidden

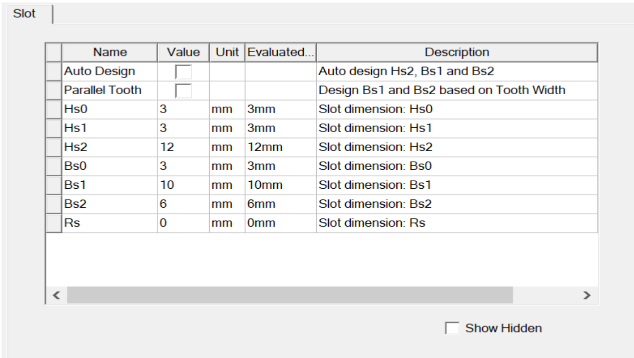

Slot

Name	Value	Unit	Evaluated...	Description
Auto Design	☐			Auto design Hs2, Bs1 and Bs2
Parallel Tooth	☐			Design Bs1 and Bs2 based on Tooth Width
Hs0	3	mm	3mm	Slot dimension: Hs0
Hs1	3	mm	3mm	Slot dimension: Hs1
Hs2	12	mm	12mm	Slot dimension: Hs2
Bs0	3	mm	3mm	Slot dimension: Bs0
Bs1	10	mm	10mm	Slot dimension: Bs1
Bs2	6	mm	6mm	Slot dimension: Bs2
Rs	0	mm	0mm	Slot dimension: Rs

Show Hidden

Fig 5 - Stator configuration

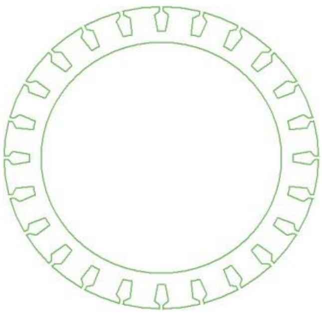

Fig – 4 Schematic overview of an outrunner brushless machine

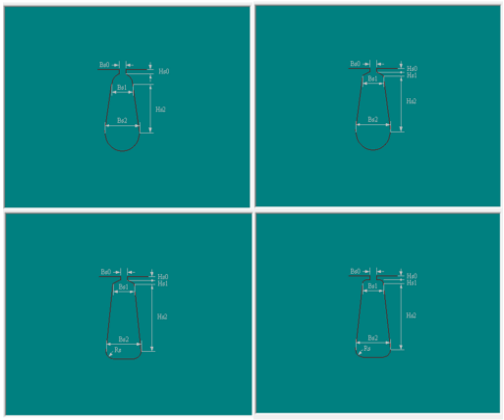

Fig – 6 : Different types of Slots

12. CIRCUIT DESIGN:

The outline of the machine is first characterized using Ansoft Rmxprt sub package. The machine has been designed here for optimal values for stator, rotor, permanent magnets, core material and winding configurations. Since as per the requirement, the power required for 2200 rpm of the machine is about 12kW, the current density should be sufficiently high inside the slot windings for the expected power output. The current density and electrical loading on the machine can be increased by increasing the number of turns and armature current in the slot windings or alternatively, by reducing the slot size and increasing the no. of Slots in stator. Since increasing the no. of turns increases the excitation current required, the slot size has been optimized for an acceptable input phase current value as shown in the relation. The Figure 5.2 shows the selected stator configuration with given dimensions.

Stator has been subjected to dual layer whole coiled type winding with respect to available stator slot area. The automatic design option by the software has been utilized for creating the number of strands and conductors per the slot to be used for design. Since the design has 20 poles and 24 slot counts, unit coil pitch has been selected. The final winding configuration used for the machine was described in below figure.

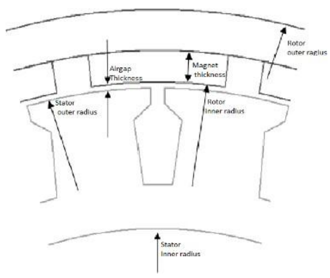

Fig -5:Stator configuration

Rotor

Name	Value	Unit	Evaluated...	Description	Read-o...
Outer Dia...	249	mm	249mm	Outer diameter...	
Inner Dia...	222	mm	222mm	Inner diameter ...	
Length	60	mm	60mm	Length of the r...	
Steel Type	JFE_Steel_SuperCore_10JNEX900_2DSF0.950			Steel type of th...	
Stacking ...	0.95			Stacking factor...	
Pole Type	1			Pole type of th...	

Show Hidden

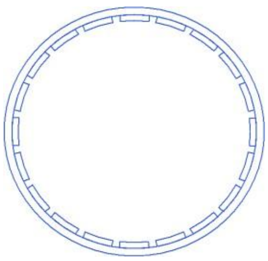

Fig – 6: Final Widing Configuration

The rotor core material selected was same as the stator lamination material, and has a stacking factor of 0.95. The advantage of exterior rotor machines is that the inertia can be adjusted by adding additional material to the rotor as per the application requirement. Since aerospace applications requires the higher torque and speed requirements, the motor inertia will be of an importance. As the earth Magnets like Neodymium Iron Boron or Samarium COBALT Magnets has higher energy density properties they have been chosen as a primary preference for the application. Since NdFeB has lower curie temperature and hence lower operating thermal point than the requirement, SmCo28 grade magnets has been selected for rotor poles as discussed earlier.

General

Name	Value	Unit	Evaluated...	Description	Read-o...
Name	Setup4				
Enabled	✓				
Operatio...	Motor			Motor or gener...	✓
Load Type	Linear Torque			Mechanical loa...	
Rated O...	13	kW	13kW	Rated mechani...	
Rated Vo...	220	V	220V	Applied rated ...	
Rated Sp...	2300	rpm	2300rpm	Given rated sp...	
Operatin...	100	cel	100cel	Operating tem...	

Show Hidden

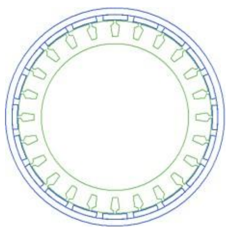

Fig – 7 : Rotor configuratio

13. SOLUTION SETUP

In reference with the of wind conditions available for an aircraft during the flight, pilot have to control the propulsion system with respect to those wind conditions. In a constant power output machine, the machine runs at constant power irrespective of the load acting on the machine, whereas in a constant speed output machine, the machine runs at a constant speed irrespective of the load acting. With reference to first case if the load acting is higher than the torque available by the machine, the machine fails to operate. Whereas in second case, for the torque available for a specific speed, if load is more, again the machine fails to operate. Hence an aircraft requires a variable torque and speed controllable propulsion system, thus, the machine is designed for linear torque output, where the torque output by the machine has linear proportionality with the speed which is controlled by operating system.

	Name	Value	Units	Description
1	Average Input Current	34647.5	mA	DC current from the source
2	RMS Armature Current	31227.3	mA	AC current through the winding
3	Armature Thermal Load	185.192	A^2/mm^3	
4	Specific Electric Loading	17349.7	A_per_meter	
5	Armature Current Density	10674100	A_per_m2	
6	Frictional and Windage Loss	16672.6	mW	
7	Iron-Core Loss	355048	mW	
8	Armature Copper Loss	271219	mW	
9	Transistor Loss	723948	mW	
10	Diode Loss	49049.4	mW	
11	Total Loss	1415940	mW	
12	Output Power	12443000	mW	
13	Input Power	13859000	mW	
14	Efficiency	89.7833	%	
15	Rated Speed	2277.65	rpm	
16	Rated Torque	52.1689	NewtonMeter	
17	Locked-Rotor Torque	1516.43	NewtonMeter	
18	Locked-Rotor Current	2047120	mA	
19	Maximum Output Power	48732800	mW	

Fig – 8: Solution setup

13. STEADY STATE PERFORMANCE

The full load operational performance output by the Rmxprt environment obtained as shown by the below figure.

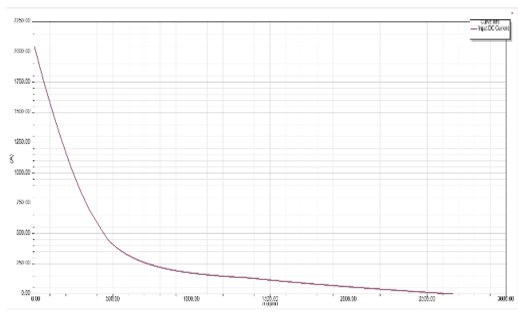

Fig – 9 : Steady state performance

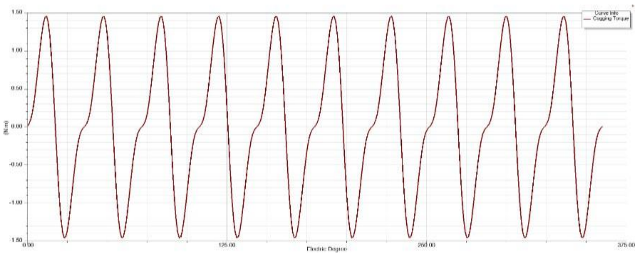

Fig – 10 : Input DC current vs Speed

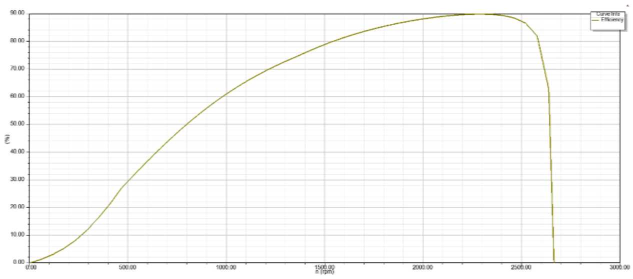

Fig – 11 Output power vs speed

14. TRANSIENT ANALYSIS

The transient analysis indicates the time dependent performance of the machine. Here the machine is analyzed for flux density distribution, flux lines torque during motion, power with respect to time, etc. The Rmxprt model is imported into Ansys Maxwell 2D environment and FEM analysis is done by assigning boundaries to the model.

Torque

The transient torque analysis is done for first 6 milliseconds. The figure below shows the torque the transient torque characteristics of designed motor.

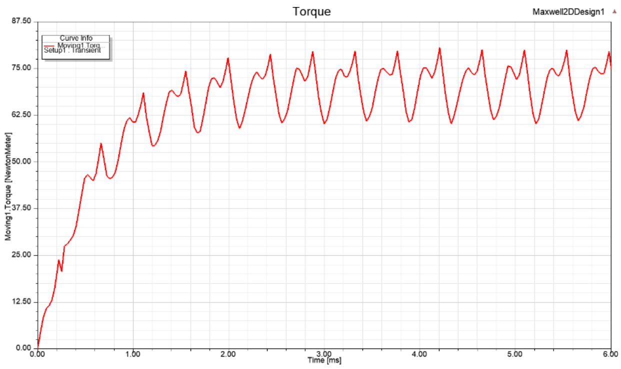

Fig – 12 : Cogging torque between two teeth

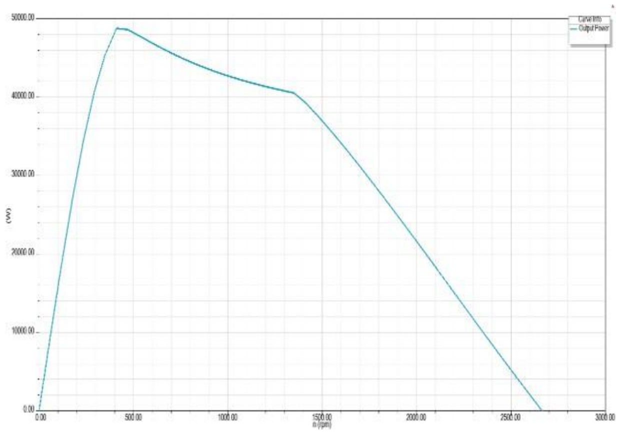

Fig – 13 : Torque with respect to time

Phase currents:

The phase current supplied and the variation of each current with time during operation is analyzed and shown below.

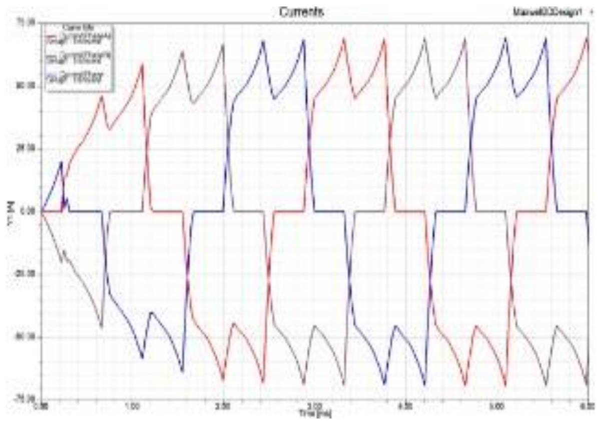

Fig – 14 : Phase current variation

Magnetic flux density:

The saturation flux density value of the selected core material is of 1.8T. whereas the maximum operating flux density among the motor parts is obtained as 1.72T. since the maximum flux density among the parts of machine is less than that of saturation flux density, the 1.72T is an acceptable value over 1.8T.

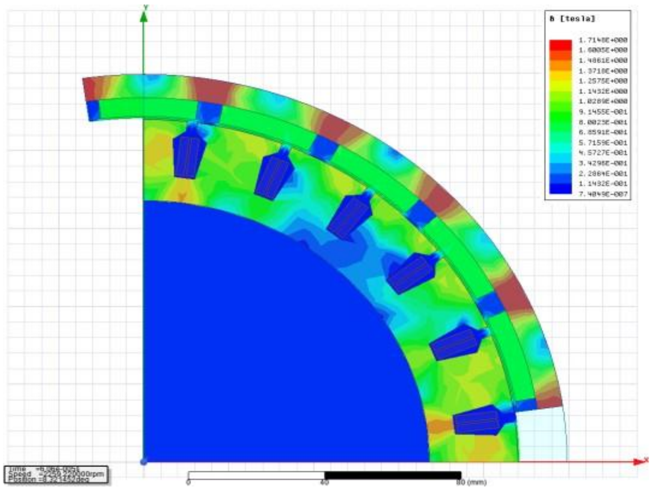

Fig – 15 : Distribution of flux density

15. PROPULSION

For the designed brushless machine, propulsion CFD analysis of the ducted propeller is conducted in this section in order to show up the advantages of motor embedded propulsion system over the shaft driven one. The torque required for both the cases were extracted through the CFD analysis and the final conclusional factors were discussed based on the results.

Analytical design of propeller

A simple ducted propeller without any guide vanes as shown is designed by using blade element moment theory and stage velocity triangles. A python program is developed based on this to obtain the accurate final results of the fan dimensions.

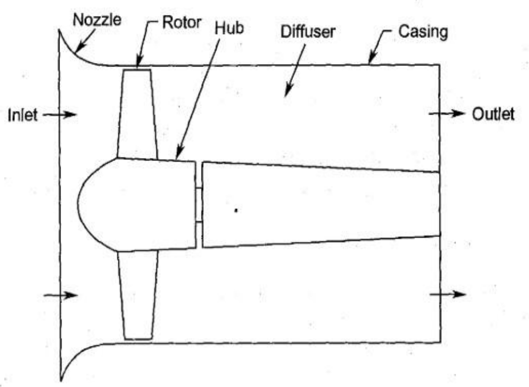

Fig – 16 : Schematic representation of a ducted fan

Stage velocity triangles

Since the intention is to design a single stage ducted propeller without any guide vanes, the construction of velocity triangles was simple. We know that in an axial fan, there are axial and swirl component of velocities were present. Since the axial component never changes throughout the rotor stage, the components C_{x2} and C_{x3} remains same and identical.

By Euler's equation, the stage work is given by,

$$W_{st} = uC_{y3}$$

And hence the power required to drive the fan is givenby,

$$P = muC_{y3}$$

Where the mass flow rate m can be obtained by,

$$m = \rho AC_X$$

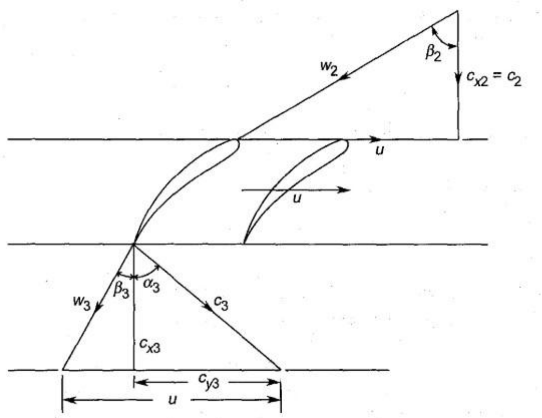

Fig – 17 : Stage velocity triangles

Python computer program

A computer program is developed in python 3.8 interface in order to design an efficient propeller blade with respect to expected hub diameter. The code uses blade element moment equations, force equations and constraint equations to accurately design any propeller blade for a ducted propeller.

```
Importing the numpy as np
From the scipy.integrate import quad


def initn():
```

```
    bl0 = [Rh]
    b = np.linspace(Rh, R, 5)
    [bl0.append(b[i]) for i in range(1, len
(b))]
    r = np.array(bl0)
    print('\nRadial position ->', bl0)

    A = np.pi*((R**2)-(Rh**2))

mdot = rho*A*V
    u = (np.pi*n/30)*r
    vt = Preq/(mdot*u)

    MomentumEqns(rho, V, r, vt, u)


def MomentumEqns(rho, V, r, vt, u):
    dltp = rho*vt*(u-(vt/2))
    a = vt/(2*u)

    T1 = 2*np.pi*r*dltp
    Qr = 2*np.pi*rho*r*V*vt
    ForceEqns(V, u, a, rho, r, vt)


def ForceEqns(V, u, a, rho, r, vt):
    phi0 = []
    K = r*vt
    BG = 2*np.pi*K
    phir = np.arctan(V/(u*(1-a)))
    phi = np.degrees(phir)+3
    [phi0.append(phi[i]) for i in range(0,
len(phi))]
    print('Section blade angle ->', phi0)

    L1 = BG*rho*u*(1-a)/np.cos(phir)
    Qr1 = L1*np.sin(phir)
    T11 = L1*np.cos(phir)
    a = K/(2*r*u)

    Constraint(n, V, R, Rh, r, K, a)
    Geometry(V, K, u)
def Constraint(n, V, R, Rh, r, K, a):
    eff0 = []
    ndr = r/R
    ndr0 = Rh/R
a0 = a[0]
```

```
    ohm = (np.pi*n/30)
    J11 = lambda ndr: 4*ohm*ndr/(V**2)
    I11 = lambda ndr: 4*ohm*ndr*(1+a0)/(V**
2)
    I21 = lambda ndr: 4*ndr*ohm*a0/(V**2)
    J10 = quad(J11, ndr0, 1)
    I10 = quad(I11, ndr0, 1)
    I20 = quad(I21, ndr0, 1)
    J1 = J10[0]
    I1 = I10[0]
I2 = I20[0]

    j = V/(2*(n/60)*R)
    Pc = K*J1
    Tc = (K*I1)-((K**2)*I2)
    T = Tc*(rho*(V**2)*np.pi*(R**2))/2
    P = pc*(rho*(V**3)*np.pi*(R**2))/2
    eff = (T*V)/P
    [eff0.append(eff[i]) for i in range(0,
len(eff))]


def Geometry(V, K, u):
    c0 = []
    W = np.sqrt((u**2)+(V**2))
    Wc = (4*np.pi*K)/(Cl*B)
    c = Wc/W
    [c0.append(c[i]) for i in range(0, len(
c))]
    print('Sectional chord ->', c0, '\n')


rho = 1.23
V = 40
n = 2260
Rh = 0.13
R = 0.5
Cl = 0.7
B = 5
Preq = 12000
initn()
```

The propeller was designed based on the above developed program which is oriented with the designed outrunner machine of 12kW. And the designed propeller vane has 92.8% efficiency. The design dimensional parameters were listed below.

Radial position (m)		Section blade angle (deg)	Sectional chord (m)
0.13		60.63	0.1001
0.2225		41.94	0.07641
0.315		31.948	0.05972
0.4075		25.89	0.04839
0.5		21.885	0.04045

Table - 5 : Propeller dimensions

16. SOLAR PROPULSION

Principle

Solar panels, which can be various sections like wings or surfaces, are nothing more than the composition of solar cells coupled in a certain or correct arrangement (fuselage, tail part etc.,). Here, during the day, the conversion of solar light into electrical energy depends on the Sun's irradiance and the slant of the light rays.

The converter, also known as the Highest Power Point Tracker, will make sure that the solar panels connected to the aircraft wing are producing the maximum amount of power. This electricity is first made available to the onboard electronic systems and the propulsion system, after which the battery will be charged using the excess energy (required for backup).

And since the solar panels are no longer producing power during the night or when there is insufficient sunshine (dull or gloomy weather), the batteries are then used to power the various components on board the aeroplane.

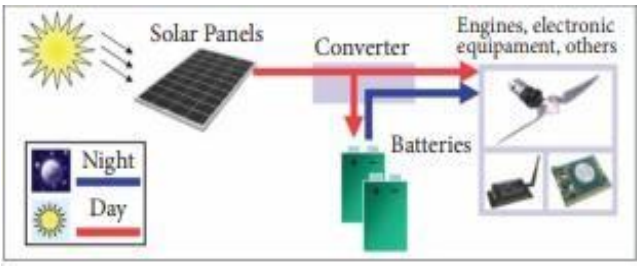

Fig - 18 : Working principle of Solar aircraft engine.

Fuel Cells

Since both batteries and fuel cells store energy in the form of reactants and generate power through electrochemical processes within the cells, this is not surprising. The fuel cell stores one or both of its reactants outside, whereas a battery stores energy and generates electricity inside of a sealed enclosure (externally). By using a fuel cell, we can expand the energy capacity of a system and do so simply by adding more fuel as needed.

During the night, the fuel cell produces electricity and water by combining the gases of oxygen and hydrogen in a regulated reaction. And during the day, the electrolytic cells recharge the system by electrolysis—the process of converting the same water into hydrogen and oxygen gases that are then stored under high pressure in tanks in the wings of the aircraft—to regenerate the system. On a daily basis, these reactants are recycled. Regenerative fuel cells are one name for this kind of technology. Additionally, a novel system design can be created that uses different electrochemical cells to produce electricity and electrolyte water, or it can use the same cells to accomplish both tasks (at a very small sacrifice in efficiency). The other type is a unitized regenerative fuel cell, which is a reversible device.

Scope

The main scope is to design and developing the low-cost unmanned HYBRID aircraft propulsion (electric-solar) airplane**s** to carry out science missions like atmospheric studies and communication support, common or military observation and for the observation missions.

17. DESIGN AND MODELLING

Design: Catia V5 is used to design the solar aircraft engine.

Fig – 19 Engine rear part.

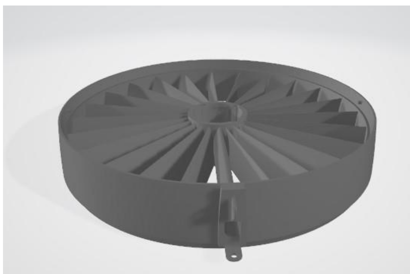

Fig – 20 : Engine mid-section part.

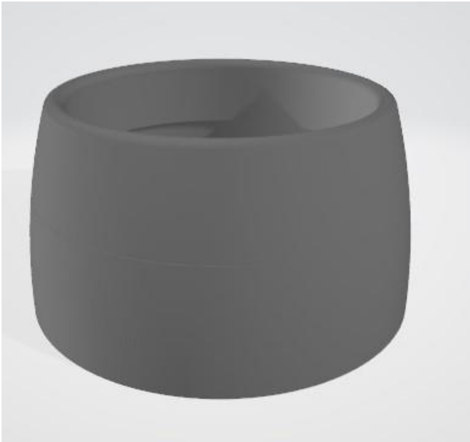

Fig – 21 : : Engine outer casing.

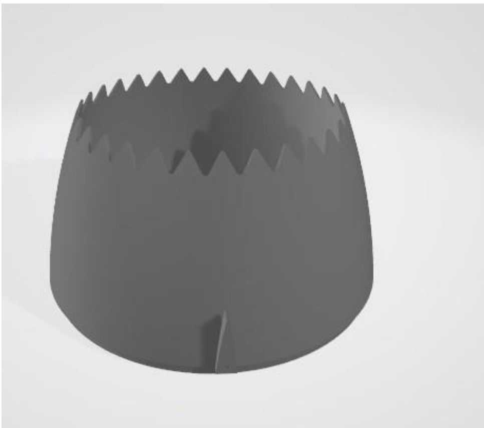

Fig – 22 : : Nozzle part.

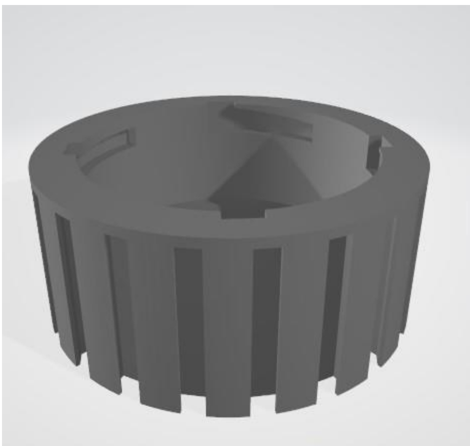

Fig – 23 : Rotor Shaft.

18. MODELLING

Modelling is done using 3D Printing technology.
Working hours was around 400 hours.

3D printing method:

A digital file can be used to create three-dimensional solid things using the 3D printing technique. An additive process is used to create a 3D-printed object. In this additive technique, material is layered on top of one another until the desired thing is constructed.

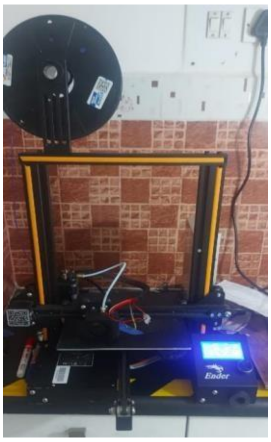

Fig – 24 : 3D Printer.

3D printing procedure:

Firstly, the Catia file/ design file is opened in the software called Ultimaker Cura 5.0.0

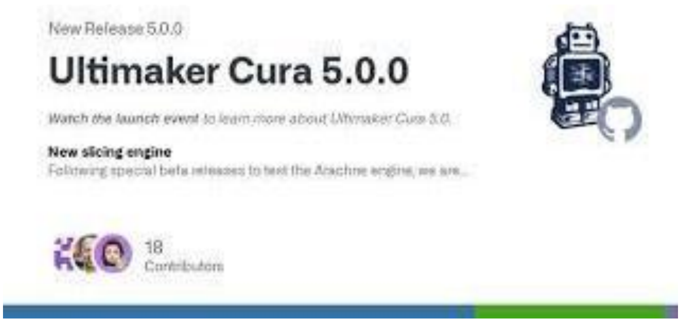

Slicing: there is an option in the software Ultimaker which converts the Catia file .STL format into G-Code.

Slice = Conversion to G code.
Then the **G-code** is opened in 3D printer by connecting with SD Card.

Then the filament is given to feed,

Filament used is PLA, PLA plus, PLA pro etc. (Polylactic acid)

An entirely biodegradable thermoplastic polymer made of renewable basic materials, PLA. PLA is one of the more widely used additive manufacturing filament materials out of the many 3D printing materials.

Fig – 24 :: PLA filament

Temperature : 200 TO 220 degree Celsius

Nozzle measure/thickness: 60 to 70

Fig – 25 : Intern Setting up the conditions for Printing

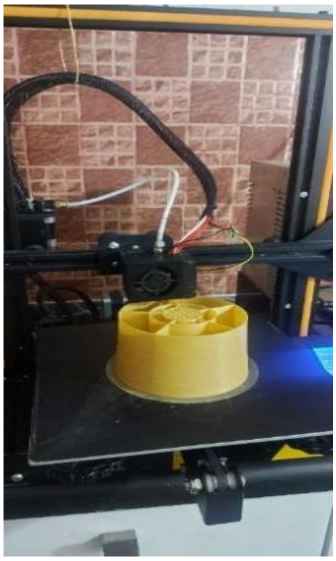

Fig - 26

Fig - 27

Fig - 28

Fig - 29

Fig - 30

Fig - 31

Fig - 32

Fig 25-32 : 3D printed engine parts

Fig 33: 3D Printed engine model assembly.

19. TORQUE COMPARISON

The ducted propeller with different driving configurations were computationally analyzed with a specific flow condition to get the torque required in driving the whole Sys. Then by observing the motor performances required by both the designs, the conclusion about efficient configuration is approached.

The CFD analysis of the designs were done in SOLIDWORKS Flow Simulation environment. The flow conditions and propeller dynamic characteristics were kept identical during analysis for both design configurations

20. PROPELLER DRIVE CONFIGURATIONS

The propeller is designed with two configurations. One is to derive the propeller through shaft and another design contains embedded outrunner motor. Then it is analyzed for required torque by driving through shaft and also as embedded motor configuration.

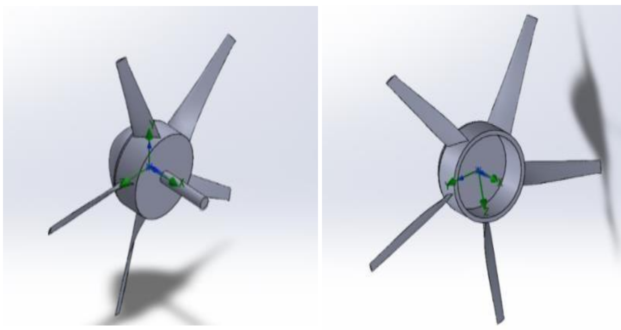

Fig - 34: Shafted and shaftless design

Shaft driven propeller

The ducted propeller designed was analyzed computationally to obtain the accurate torque required to drive the whole system.

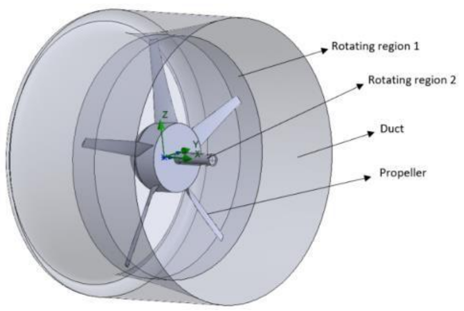

Fig – 35 : Computational domain - Shaft driven fan

The propeller is analyzed for a flow laminar and turbulent flow conditions. Since the torque required depends on the turbulence of inlet flow field, a higher turbulence factor is introduced to get accurate torque value as shown in below table (If the turbulence is higher, the resistive torque required for the propeller is also higher).

Turbulence intensity	Turbulence length (m)	Angular velocity (rad/sec)
15%	0.8	900

Table- 6 : Free stream conditions

In this case, since the propeller is to be driven through a shaft connected to a motor, an additional mass of the shaft has to be considered in between the propeller hub and the rotor of the motor. This increases the inertia of the whole propeller – shaft set but it also reduces the contribution of the inertia with torque since the shaft diameter is less compared to hub diameter and contribution of rotational inertia depends on the diameter of component. The below table shows the torque required to drive the propeller in mentioned specific flow condition. This torque requirement increases as the shaft diameter get increased due to increase in volume and mass.

namee	Unitts	Valuees	Progress	Criteriaa	deltails	Use in convergence
GG Maximum total of Pressure 1	Pa	2315 72.2 4	100	35944 .9006	8470.4 6065	On
GG Force (X) 3	N	- 635. 732	100	1163. 24671	364.38 848	On
GG Torque (X) 4	N * m	- 43.0 08	100	5.078 60295	5.0752 943	On
GG Torque (Y) 5	N * m	- 28.1 94	100	19.34 02465	10.286 5316	On
GG Torq ue (Z)6	N * m	16.1 13	100	15.43 17377	9.6397 8628	On

Table – 7 : Result - Shaft driven propeller

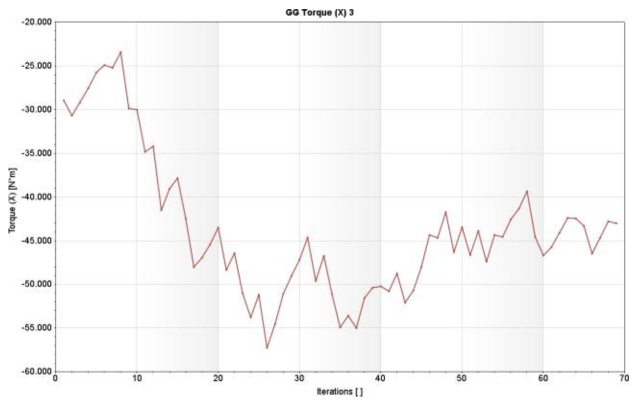

Fig – 36 : Torque demand – Shafted propeller

Motor embedded propeller

Since there is no shaft present in the motor embedded configuration, the only rotating region is the propeller with a hollow hub.

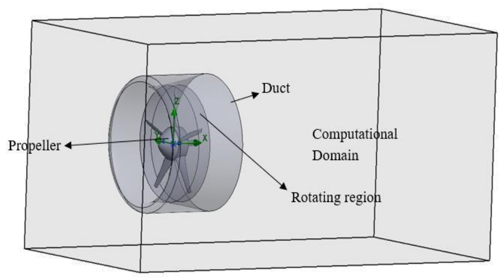

Fig - 37: Computational domain – Shaftless propeller

As in the previous shaft driven condition, the flow field conditions were taken identical in order to compare the torque requirement demanded by both the conditions easily.

Turbulence intensity	Turbulence length (m)	Angular velocity (rad/sec)
15%	0.8	900

Table – 8 : Freestream conditions

In this case, since there is no shaft is introduced to drive propeller, only the mass of hub and rotor contributes for the inertia. Also because of the absence of shaft or gear box, the mass and volume of the whole system get reduced. Due to reduction in this mass and volume, torque required to overcome the inertia is also get reduced. And hence the torque demand by the propeller is lower compared to previous shaft driven case.

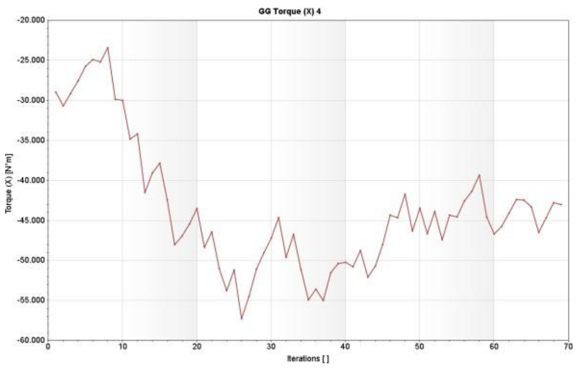

Fig – 38 : Torque demanded - Shaftless propeller

Comparing to previous case, in this condition, the propeller hub is directly driven by the rotor of outrunner motor. When driving a shaft, due to the fact that the shaft diameter is smaller than the propeller hub, the contribution of inertia with torque is less. But while considering this case, since the hub is directly driven by rotor by embedding the whole motor inside, the contribution of inertia is more for torque due to larger diameter of the hub.

name	Units	Values	Pro gress	Criteria	delta	Use in convergence
(X)GG Torque	N*m	- 41.3 69	100	4.240 0954 2	4.176 60895	On
GG Maximum Total Press ure 2	Pa	2295 98.5 8	100	3338 1.863 2	7870. 62764	On
GG Forc e (X) 4	N	222. 681	100	1410. 3670 5	366.2 45403	On
GG Torque (Y) 5	N*m	- 4.32 3	100	17.10 1270 4	7.618 50285	On
GG Torque (Z) 6	N*m	3.78 6	100	24.89 9388 2	9.352 42397	On

Table – 9 : Result - Shaftless propeller

21. PERFORMANCE

At final the difference in the performance and characteristics of both shafted and motor embedded techniques were compared and discussed in this section. Based on the performance comparison, the suitable technique for different aircraft applications will be discussed considering the previous results.

Volume reduction

A shafted engine may include some couplers, sometimes gear box or may need specially designed shafts for some drives. This arises a rise in overall volume and hence the weight of the entire propulsion system. Where as in the shaftless, motor embedded propulsion system, the volume is reduced, since the propulsion system consist of only a hub propeller driven by embedded motor.

Torque requirement

The torque required to drive a propeller during flight is an important factor. This torque requirement is directly depending on inertia of the rotating regions as shown by equation below.

$$T = I\alpha$$

Where 'T' is the torque required, 'I' is the moment of inertia and 'α' is called angular acceleration. Since the shafted propulsion system has more components than a shaftless one, the inertia of the propeller is more. Because of this higher inertia, the torque required to drive the propeller becomes greater compared to shaftless one.

The moment of inertia depends on the mass and diameter of the rotating shaft or region. Illustratively, for a solid rotating disc having of radius of 'r' and it has the Mass 'M', then the moment of inertia will be given,

$$I = \frac{1}{2}Mr^2$$

This sets a constraint such that, for a shafted propulsion system since the shaft has some radial dimension and mass, this introduces some additional inertia to the propeller hub, which has to be overcome by the certain torque by motor.

Observing the results of shafted propeller, the average torque required by the propeller is of 43 Nm. Whereas for a motor embedded shaftless propulsion, the required torque is of 41.37 Nm for same freestream conditions. This says that the torque required for a shaftless propulsion system, the torque required is significantly less compared to a shafted propulsion system. This is because the shaft introduces an additional moment of inertia which has to be overcome by the torque supplied by motor.

Contribution of inertia

The torque is an important factor during flight to resist the variational freestream loads acting on propeller vanes to provide specific thrust at given rotational speed of the propeller. This says that to provide higher resistive torque for propeller, inertia of the propeller should be more so that contribution of inertia in this resistive action is enhanced. At the same time, the weight of the propulsion system should be reduced in order to increase flight performance.

Since the inertia depends on the product of mass and radius of the rotating region, the contribution of inertia can be increased by introducing a large hollow hub rotating region as in the case of shaftless motor embedded propulsion.

When the shafted propulsion is considered, the additional mass of the shaft introduces a lesser contribution of inertia with torque because of the smaller radial dimension of the shaft. This causes a less thrust output for given torque and rotational speed compared to shaftless propulsion technique. Since, in the shaftless technique, the hub of the propeller is hollow and the embedded rotor of the motor is direct contact with hub, the radius of the hub is increased. This reduces the torque required and allows the propeller rotational speed to more effectively act upon the incoming freestream thereby increasing the total performance of the entire propulsion. This can be compared by the results given below.

Property	Shafted propeller	Shaftless propeller
elocity(m/s)	27.14	30.791
Total thrust (N)	201.918	309.542

Table – 10 : Output Comparison

CONCLUSIONS

The whole study is oriented towards realizing the best possible way to propel a lightweight and solar powered electric aircraft. The performed observations concludes that an outrunner motor embedded propulsion system provides more ease propulsion by considering following aspects.

1. The motor with interior rotor can only drive a propeller through a shaft, whereas a motor with exterior rotor can be embedded inside the hub of a propeller, more likely in a ducted propeller thereby reducing weight and volume of the entire propulsion system.

2. An exterior rotor motor can have smaller volume than an inrunner motor for same torque output. This reduces sufficient mass of copper windings and core steel material and hence opens door for more ease propulsion techniques for lightweight electric aircrafts.

3. The inertia of the motor can be maintained by adding or removing the material in the hollow hub of propeller. This allows for capability to design the propulsion system for a required inertial contribution.

4. Since the propeller consist of larger hub diameter with hollow structure, this helps in higher contribution of inertia towards variable freestream loads during flight by maintaining constant propeller speed.

5. The only disadvantage is that the required starting time of the engine due to higher inertia of the hub, since the inertia of mounted vanes also should be considered, the starting time of the engine may delay.

6. This delay in staring time of the motor restricts this embedded motor configuration for highweight aircrafts. However, this configuration is more likely suitable for solar propelled aircrafts because of above advantageous characteristics and thus this configuration is introduced as 'magneto propulsive solar engine'.

REFERENCES

1.University of Dunaujvaros, "Electric aircraft - present and future," H-2400 Tancsics-Mihaly-utca 1, Hungary, 2019. Andras Nagy

2.Review of Maglev Train Technologies by Ki-Chan Kim, Hyung-Woo Lee, and Ju Lee was published in the IEEE Transactions on Magnetics in 2006.

3. Electrical Engineering Department, Maulana Azad National Institute of Technology (MANIT), Bhopal, India, "Electrical Components of Maglev Systems: Emerging Trends," article published in 2019.

4. "Design and Prototyping Methods for Brushless Motors and Motor Control," Shane W. Colton, Department of Mechanical Engineering, Massachusetts Institute of Technology, 2010, partial fulfilment of the requirements for the degree of MS in Mechanical Engineering.

5.International Journal of Technical Research and Applications, "Solar Powered Aircraft," Shubham Patil, Rajdeep Jagdale, Pratik Thakur, and Sar, 2016.

6."Design and Prototyping of 3-Phase BLDC Motor," by Y.B. Adyapaka Apatya, Aries Subiantoro, and Feri Yu, Electrical Engineering Department, Universitas Indonesia, Indonesia, 2017.

7.Devaiah Nalianda, propulsion Engineering Center, Cranfield University, Bedfordshire, UK, 2016. "Review of Modern Low Emissions Combustion Technologies for Aero Gas Turbine Engines."

8."Design of an outer-rotor brushless dc motor for control moment gyroscope applications by N. Cagan," Middle East Technical University's degree programme in natural and applied sciences, 2015.

9.IET Electric Power Applications, Vols. doi: 10.1049/iet-epa.2017.0639, no. 13, 2018. X. Zhang, "Large electrification machines for aviation electric," Department of Electricaland Computer Engineering, University of Illinois, Urbana-Champaign, 306 N. Wright Street, Urbana, IL 61801, USA.

10. Computer-Aided Design of a Brushless DC Motor with Exterior-Rotor Configuration, National Yunlin University of Science & Technology, Vols. 10.3722/cadaps.2012.457-469, no. CAD Solutions, LLC (2012), http://www.cadanda.com, p.

11. 1994 issue of the propulsion and power magazine, "Designing of Optimum Propellers."

12. Design and analysis of single and dual rotation ducted fans, G. S. Page, 34th Aerospace Sciences Meeting and Exhibit, Reno, NV, Jan. 15–18, 1996, Vols. AIAA Meeting Papers on Disc, January 1996, no. AIAA inc., 1996.

13. Contra-rotating Ducted Fan Aerothermodynamic Design Procedure for Unmanned Applications, A. F. Nemnem, Cairo, Egypt: Military Technical College, Aerospace Engineering Department, vol. 322309589, no. AIAA, 2018.

BIOGRAPHIES

Mr. Chandrashekar
Presently, P.G. Student,
Department of Aerospace Propulsion Technology, VTU-CPGS Bengaluru Region, VIAT, Muddenahalli, Chikkaballapura, Karnataka, India.

Dr. Chikkanna N
Associate Professor & Chairman,
Department of Aerospace Propulsion Technology, VTU-CPGS Bengaluru Region, VIAT, Muddenahalli, Chikkaballapura, Karnataka, India.

Mr. Sanjeev G Palekar
Assistant Professor
Department of Aerospace Propulsion Technology, VTU-CPGS, Bengaluru Region, VIAT, Muddenahalli, Chikkaballapura, Karnataka, India.

Mr. Prashanth Radhakrishnan
Director – Aerospace R & D
Dautya Aerospace
Bengaluru, Karnataka, India.